Published version available at: https://doi.org/10.1016/j.combustflame.2022.112348

Flame stabilization in narrow channels by a highly conductive wall segment: application to small-scale combustion devices

Vadim N. Kurdyumov [1], **Carmen Jiménez**

Department of Energy, CIEMAT, Avda. Complutense 40, 28040 Madrid, Spain

Abstract

The structure and dynamics of premixed flames in narrow channels in the presence of a highly conductive wall segment are investigated in this work. It is shown that these systems present a multiple steady-state regimes. A linear stability analysis applied to these steady solutions reveals that several steady-state solutions may be simultaneously stable. The stability analysis results are confirmed by time-dependent simulations, that show that the actual realization of one or another stable regime depends on the initial conditions. Finally, we show that nonlinear periodic and chaotic dynamics may appear under certain conditions in these system.

1 Introduction

One of the main issues in the design of combustion devices is to guarantee flame stabilization and thereby the stable operation of the system. It is well known that with a decrease in the size of the device, heat losses increase, and this can result in destabilization of the system operation and even extinction of the flame. On the other hand, reducing the size of the device, for example, reducing the width of a channel in which the combustion process takes place, makes it possible to reach by heat recirculation a temperature that is higher than the adiabatic flame temperature, an effect widely used in small-scale combustion systems, see various reviews [1–4]. This becomes extremely important for burning mixtures with low chemical-energy content which cannot be burnt without additional external heating.

One of the most commonly used configurations to achieve this heat recirculation effect is a device consisting of parallel channels with heat exchange between them. The reactant mixture flow in adjacent channels is usually organized in opposite directions, that is, as counter-current channels. From the earliest works, proposing this kind of arrangement almost fifty years ago [5–7], this idea was developed extensively later, using analytical and numerical methods [8–12].

[1]Corresponding author

In such designs the material chosen for the separating wall should be carefully chosen to ensure an adequate heat exchange rate between channels. The required wall thermal properties depend on operational characteristics, such as the total flow rate of the combustible mixture, its energy content, the operational combustion temperature and others.

It should be noted that the thermo-physical properties of the channel walls have a fundamental influence on the structure and dynamics of the flame burning inside it, particularly for small channel widths. When modeling small-scale devices, the role of the wall is often limited to transferring heat from one channel to the next. Heat transfer is often considered only in the direction transverse to the channel, which implies considering the rate of heat exchange between channels as proportional to the temperature difference between them [9,10,12]. In general, this approximation is valid for sufficiently thin walls, as confirmed within the framework of asymptotic analysis [11].

However, another situation is also possible, when the thermal conductivity of the wall is so high that the temperature inside the wall is close to be uniform (and even asymptotically constant, to a first approximation). When parallel channels are connected by a wall of this kind, the wall acquires the additional role of heat accumulator and works as a flame holder.

The assumption of temperature homogeneity within a solid material constituting the combustion device due to its high thermal conductivity has been widely used before. Models for the combustion process in a porous layer can serve as examples [13–17]. This approximation was recently used the same way in [18]. Another example would be a high thermal conductivity solid bluff-body used to stabilize a flame in a stream of reactant mixture [19,20].

The condition of temperature homogeneity in a solid is formally obtained by a rigorous (regular) mathematical expansion in terms of a small parameter (the ratio of the thermal conductivities of the gas and the solid), if all other dimensionless quantities are formally taken to be of the order of unity. Of course, situations are possible when another parameter is just as small, for example, the ratio of the wall thickness to the width of the channel. Then, due to the presence of two small parameters in the problem, the final asymptotic formulation depends on the value of their ratio.

It is interesting to note that in almost all the above examples, the homogeneity of temperature within a solid body (or part of it) leads to the appearance of the phenomenon of multiplicity of steady-state solutions for the combustion field. This is due to the strong nonlinearity of the problem arising from the interaction of a flame with a heated body. However, as shown in [10,21,22], the condition of temperature homogeneity in the solid part of a combustion device

is by no means necessary for the phenomenon of heat recirculation and multiplicity of steady-state solutions.

The effect of the interaction of a wall with a flame has been studied extensively in the past [23–31], both experimentally and numerically, and more recently in [32, 33]. In the mentioned recent studies the conjugated heat transfer between the gas and the solid walls was solved. On the other hand, the flame was stabilized relative to the channel walls by adjusting the flow rate: the flame heats the wall, and the wall contributes to stabilization by preheating the fresh gases, but flame stabilization was obtained for a unique flow rate value. This distinguishes the situation considered in [32, 33] from that of the present study, in which a steady-state flame can be obtained within a continuous interval of the flow rate.

In the present work, we assume that the walls are adiabatic except for a segment of finite length which has high thermal conductivity. Although the study is done mainly focusing in the case of a single channel, this simplified configuration is directly related to the operation of a small scale device consisting of a series of channels. The main purpose of this study is to investigate the flame stabilization effect by a highly conductive wall acting as a flame holder.

2 Formulation

Consider a planar channel of width H through which a combustible mixture flows with an initial temperature T_0. The channel walls are assumed to be thermally adiabatic, with the exception of a segment of length L made from a material of high (asymptotically infinite) thermal conductivity. A sketch of the problem is given in Fig. 1 (A). The high thermal conductivity of this segment acting as a flame holder results in its constant temperature, T_w, which must be found as a part of the solution. Anticipating the asymptotic formulation of the problem, it will be assumed that the wall thickness is of the same order as the channel width.

The assumption of high conductivity allows us to consider the configuration of Fig. 1 (A) as a part of a more general combustion device consisting of a series of parallel channels interacting thermally with each other through the highly conductive wall segments, as shown in Fig. 1 (B). It is obvious that the direction of the flow in each channel does not play a significant role, since the thermal interaction takes place only through the wall segments of constant temperature. Assuming that the channels are identical, with the same mixture flow rate in each of them, the problem can be reduced to one channel (in a certain sense).

A simple estimate indicates that the condition of (infinitely) high thermal conductivity of

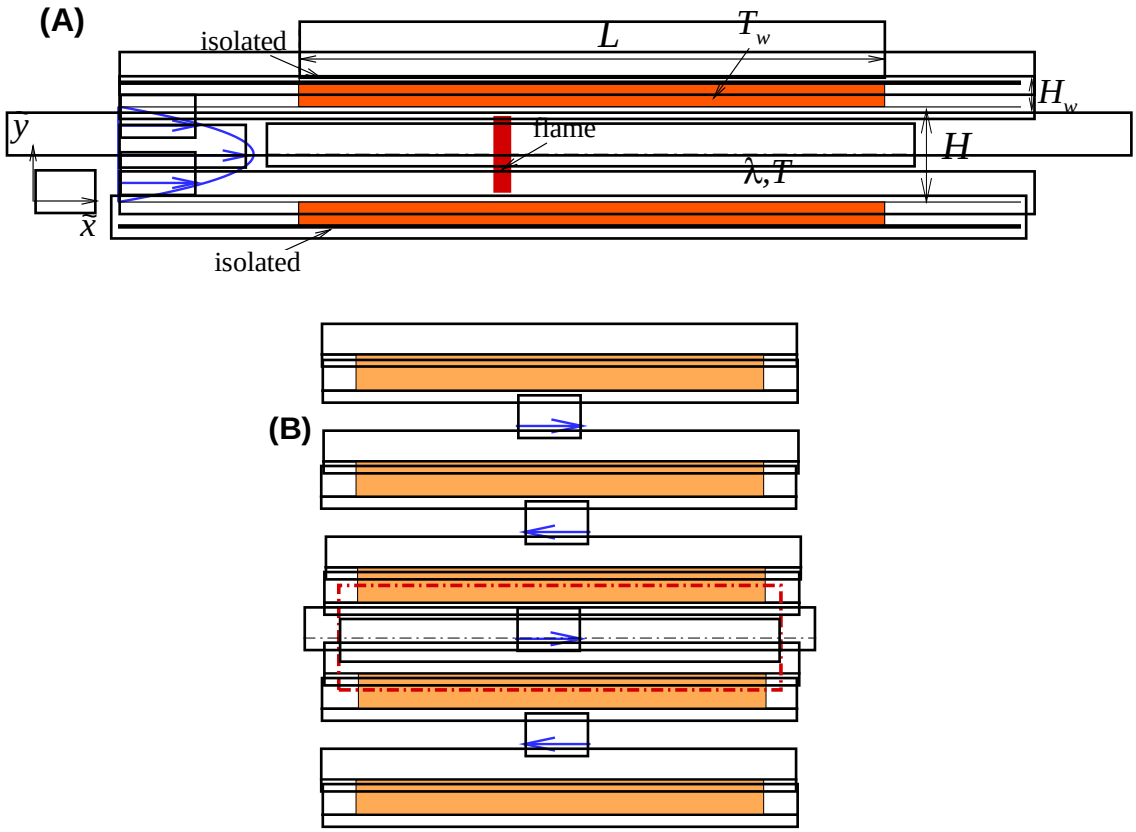

Figure 1: Sketch of the problem: (A) a single channel and the coordinate system; (B) the corresponding system of parallel channels in which only a single channel is considered (the region indicated by a dotted line).

the channel walls can be easily achieved in practice. For example, the thermal conductivity of metal-like materials or silicon carbide is of order $10^2\, W/mK$ while the thermal conductivity of gases is only a fraction of $1\, W/mK$. The temperature dependence of these quantities does not change the essence of the matter.

It is assumed that the mixture has a deficient component (fuel or oxidizer) and changes in the non-deficient mass fraction by chemical reaction remain small. The chemical reaction in the gas phase is modeled by a global irreversible step of the form Fuel + Oxidizer$\rightarrow$ Products + Q, where Q is the total heat of combustion per unit mass of deficient component. Then, assuming that the reaction is first order with respect to each of the reactants concentrations, the reaction

rate takes the form $\Omega = \mathcal{B}\rho^2 Y e^{-\mathcal{E}/\mathcal{R}T}$, where Y is the deficient reactant mass fraction, $\mathcal{E}$ is the overall activation energy, T is the temperature, $\mathcal{R}$ is the gas constant, and $\mathcal{B}$ is the appropriately defined pre-exponential factor. For example, Ω stands for the oxidizer consumption rate in rich mixtures.

For the sake of simplicity, this work adopts a diffusive-thermal model, according to which the density of the mixture, ρ, the heat capacity, c_p, the thermal conductivity, λ, and the molecular diffusivity, $\mathcal{D}$, are all assumed constant. Consequently, the flow field is not affected by combustion and the flow velocity is given by the Poiseuille flow, $U_x = 6U_0(1-\tilde{y}/H)(\tilde{y}/H)$, $U_y = 0$, where U_0 is the mean flow velocity. This study is limited to thin channels and assumes that purely hydrodynamic effects associated with, for example thermal expansion, are of secondary importance. Thus, the effects of thermal expansion and variable transport properties will be reported elsewhere.

Dimensionless parameters are based on the planar flame speed S_L and the thermal flame thickness defined as $\delta_T = \mathcal{D}_T/S_L$ (representing the thickness of a planar adiabatic and isobaric flame), where $\mathcal{D}_T = \lambda/\rho c_p$ is the thermal diffusivity. Below we use Y_0 for the initial mass fraction and $T_a = T_0 + QY_0/c_p$ for the adiabatic flame temperature. The non-dimensional temperature is defined as $\theta = (T-T_0)/(T_a-T_0)$. Similarly, $\theta_w = (T_w - T_0)/(T_a - T_0)$ is the non-dimensional wall temperature. In the following, we use the channel height H and the thermal flame thickness δ_T as the reference scales in longitudinal and transverse directions, $x = \tilde{x}/\delta_T$, $y = \tilde{y}/H$, and choose $\delta_T^2/\mathcal{D}_T$ and Y_0 to normalize the time and the mass fraction, respectively. The parameters $a = H/\delta_T$ and $\ell = L/\delta_T$ stand for the dimensionless channel width and the dimensionless length of the heat exchange segment.

Under the above conditions, the energy conservation equation and the equation for the deficient reactant mass fraction take the following dimensionless form

$$\frac{\partial\theta}{\partial t} + mv(y)\frac{\partial\theta}{\partial x} = \frac{\partial^2\theta}{\partial x^2} + \frac{1}{a^2}\frac{\partial^2\theta}{\partial y^2} + \omega\,, \tag{1}$$

$$\frac{\partial Y}{\partial t} + mv(y)\frac{\partial Y}{\partial x} = \frac{1}{Le}\left(\frac{\partial^2 Y}{\partial x^2} + \frac{1}{a^2}\frac{\partial^2 Y}{\partial y^2}\right) - \omega\,, \tag{2}$$

Here $v(y) = 6y(1-y)$ and

$$\omega = \frac{\beta^2}{2Le\,u_p^2} Y \exp\left\{\frac{\beta(\theta-1)}{1+\gamma(\theta-1)}\right\} \tag{3}$$

is the dimensionless reaction rate.

When writing below the equation for the temperature of the channel wall, we take into account possible heat losses to the external environment, $R_{ext} = h_{ext}(T_w - T_0)$, only for the case where one channel instead of a system of parallel channels is considered. Taking into account the infinite conductivity of the heat exchange segment, the wall temperature is determined by the balance equation

$$C\frac{d\theta_w}{dt} = q - b_{ext}\theta_w \,, \tag{4}$$

where q denotes the total heat flux to the wall from the gas phase,

$$q = -\int\limits_0^\ell \left.\frac{\partial\theta}{\partial y}\right|_{y=1} dx \,. \tag{5}$$

The parameters appearing in Eq. (4) are

$$C = \xi \cdot \frac{\rho_w c_w}{\rho\ c_p}\frac{L H_w H}{\delta_T^3} \quad \text{and} \quad b_{ext} = \frac{h_{ext} H}{\lambda \delta_T} \,, \tag{6}$$

where ρ_w, λ_w and H_w are the density and thermal conductivity of the wall material and the wall thickness. Here $\xi = 1/2$ if the system of identical channels is considered (because half the width of the wall must be taken into account for the thermal balance) while $\xi = 1$ for a single channel. In the first case we also have $b_{ext} \equiv 0$.

The procedure for obtaining Eq. (4) from the general equation for the temperature inside the wall is exactly the same as that presented in [20]. It consists in a regular expansion of all variables in terms of a small parameter of the ratio of thermal conductivities in the gas and the solid wall, $\epsilon = \lambda/\lambda_w \ll 1$, implying formally other parameters of order of unity. We will also consider cases with $a = H/\delta_T = O(1)$, since if a is small, the consideration is complicated by the presence of two small parameters in the problem and the resulting asymptotic equations depend on their ratio, ϵ/a.

Anticipating the results reported below, the problem given by Eqs. (1)-(2) is considered only for flames with unity Lewis number. As shown in [34], non-symmetric flames do not arise for $Le = 1$ within the framework of the constant density model. Thus, the computing domain is reduced to $1/2 < y < 1$. Results for non-unit Lewis numbers, when the appearance of non-symmetrical flames is possible, will be reported elsewhere.

The appropriate boundary conditions for the gas temperature and the deficient mass fraction become

$$y = 1/2, \quad \forall x: \quad \partial\theta/\partial y = \partial Y/\partial y = 0 \,; \tag{7}$$

$$y = 1, \quad \begin{cases} 0 < x < \ell : & \theta = \theta_w, \quad \partial Y/\partial y = 0\,, \\ x < 0 \text{ and } x > \ell : & \partial\theta/\partial y = \partial Y/\partial y = 0\,. \end{cases} \tag{8}$$

For the upstream and downstream boundary conditions, it should be required

$$\begin{aligned} x \to -\infty : \qquad & \theta = Y - 1 = 0\,, \\ x \to \infty : \qquad & \partial\theta/\partial x = \partial Y/\partial x = 0\,. \end{aligned} \tag{9}$$

In addition to the parameters specified in Eq. (6), the following non-dimensional parameters appear in the above equations: the Zeldovich number, $\beta = \mathcal{E}(T_a - T_0)/\mathcal{R}_g T_a^2$, the Lewis number, $Le = \lambda/\rho c_p \mathcal{D}$, the heat release parameter, $\gamma = (T_a - T_0)/T_a$ and the non-dimensional flow rate, $m = U_0/S_L$, normalized with the planar burning velocity, S_L.

The factor $u_p = S_L/U_L$ appearing in Eq. (3) has been introduced to account for the difference between the asymptotic value of the laminar flame speed,

$$U_L = \sqrt{2\rho\mathcal{B}\mathcal{D}_T Le\beta^{-2}}\exp\left(-\mathcal{E}/2\mathcal{R}T_e\right),$$

obtained for large activation energy ($\beta \gg 1$) and the numerical value S_L calculated for a finite β. The factor u_p ensures that for a given β the non-dimensional speed of a planar adiabatic flame equals one. Clearly, the factor u_p tends to one when $\beta \to \infty$. The numerical values of u_p were reported in [34] as a function of the Lewis number for $\beta = 10$ and $\gamma = 0.7$. These values are kept as representative values in the present study, unless otherwise stated.

3 Numerical treatment

Steady as well as time-dependent computations were carried out in a finite domain, $x_{min} < x < x_{max}$, where $x_{min} \leqslant -10$ and $x_{max} \geqslant \ell + 10$ were used. The size of the domain was varied in order to check the independence of the results. The spatial derivatives were discretized on a uniform grid using second order, three-point central differences. For unsteady calculations an explicit marching procedure was used with first order discretization in time. The typical time step was $\tau = 10^{-4} \div 10^{-5}$. In order to determine steady (but not necessary stable) solutions, the steady counterpart ($\partial/\partial t \equiv 0$) of Eqs. (1) and (2) was solved using a Gauss-Seidel method with over-relaxation.

The main criterion to check that the required accuracy of the results had been achieved was the value of the wall temperature. The number of grid points was varied from 601×51 to 1201×101. Figure 2 shows the changes in θ_w over time when these two grids are used,

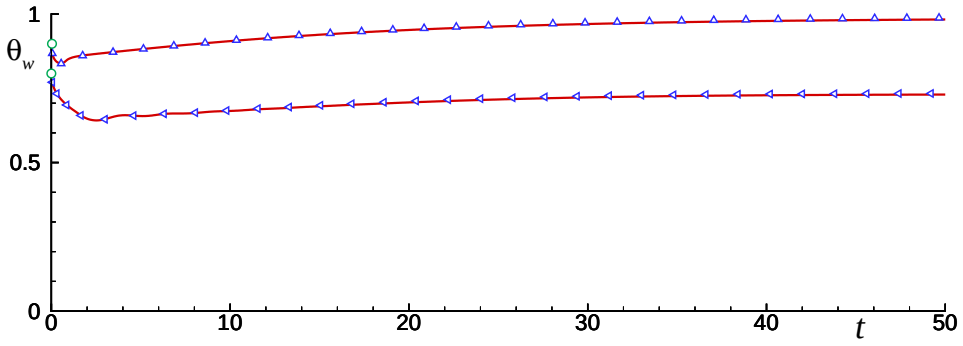

Figure 2: Comparison of numerical results for the wall temperature, θ_w, carried out on two grids, 601×51 (solid lines) and 1201×101 (triangles), for $m = 5.2$, $a = 3$, $\ell = 10$ and $C = 200$. The open circles show the initial values of the wall temperature.

represented by solid lines and symbols. Initial distributions in the gas phase were $\theta = 0$ and $Y = 1$, while the values of the wall temperature at $t = 0$ were $\theta_w = 0.8$ and 0.9 (indicated with open circles). It can be seen that there is no appreciable difference between the results obtained in the two grids. This comparison shows that the selected number of grid points and time step result in good accuracy of the results.

To find steady-state solutions ($\partial/\partial t \equiv 0$), the wall temperature θ_w was fixed. After that, the heat flux q was calculated as a function of θ_w. It is obvious that the values of θ_w for which $q(\theta_w) = b_{ext}\theta_w$ is satisfied correspond to steady-state solutions. When heat losses to the exterior are neglected, $b_{ext} = 0$, the steady state solutions are the roots of $q(\theta_w) = 0$. Note that the value of parameter C does not affect the steady-state solutions.

Summing up Eqs. (1) and (2) written for the steady-state case and then integrating over the domain, one can obtain

$$q = \frac{1}{2} m a^2 \Big(1 - 2 \int_{1/2}^{1} v(y) \big[\theta + Y\big]\big|_{x\to\infty} dy\Big)\,, \tag{10}$$

where the upstream conditions given by Eq. (9) were used. If we assume that the fuel burns out completely and the temperature is uniform across the channel outlet, Eq. (10) can be simplified to

$$q = \frac{1}{2} m a^2 (1 - \theta_{out})\,,$$

where $\theta_{out} = \theta|_{x\to\infty}$ is the outlet temperature. Thus for $b_{ext} = 0$, the constraint $q = 0$ results in

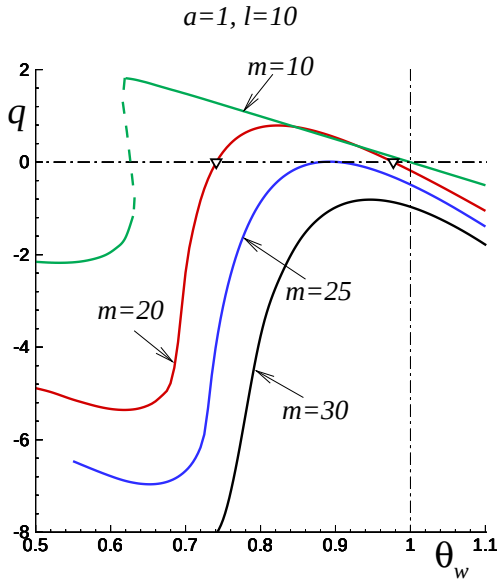

Figure 3: The response curves q versus θ_w computed for $a = 1$, $\ell = 10$, and various m. The $m = 10$ curve shows hysteretic behavior. The points shown by open triangles for the curve with $m = 20$ correspond to the flame structures shown in Figs. 4 and 5.

the outlet temperature being equal to the adiabatic temperature due to the lack of heat losses to the environment.

4 Steady-state solutions

Let us assume $\partial/\partial t = 0$ in Eqs. (1)-(2) and (4). Since the channel walls are adiabatic outside the heat exchange segment, there is a critical value of the flow rate, m_{c1}, below which the flame can propagate upstream. This critical value is determined by the flash-back condition, namely the condition when the flame does not move relative to the wall. This issue was discussed in [34], for example. It can be easily obtained that $m_{c1} \to 1$ in the limit $a \to 0$ because there is no extinction width in the adiabatic channel and the flame shape becomes planar as $a \to 0$. Finally, to prevent flame propagation upstream the heat exchange zone, $m > m_{c1}$ should be used.

Figure 3 shows the heat flux, q, as a function of the wall temperature, θ_w. All curves are calculated for $a = 1$ and $\ell = 10$. It can be seen that there are two non-trivial solutions of the equation $q = 0$ for sufficiently large values of m, e.g. $m = 20$. In addition to non-trivial solutions, there always exists a trivial (cold) solution corresponding to $\theta \equiv 0$. Thus, the total

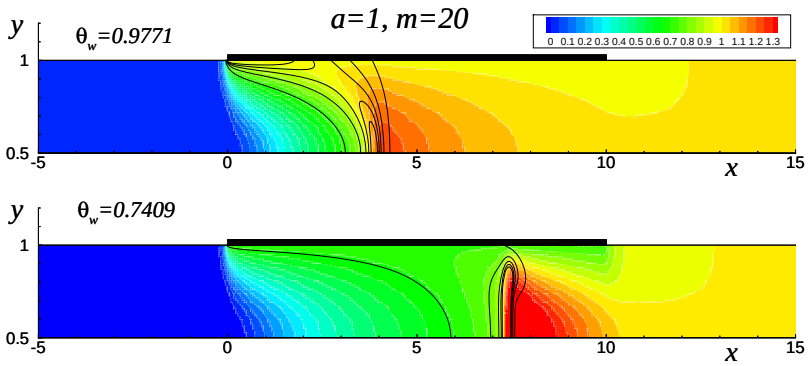

Figure 4: Flame structures corresponding to the open triangles of Fig. 3 for $a = 1$, $m = 20$ and $\ell = 10$, for the temperature (color plot) and the reaction rate (isolines at $\omega = 1$, 5, 10, 15 and 20).

number of steady-state solutions is three. It can be seen that there is a second critical value of the flow rate, $m_{c2} \approx 25$ for $a = 1$ and $\ell = 10$. At this value of the flow rate, the two non-trivial solutions merge into one, and disappear at $m > m_{c2}$. As the flow rate decreases, a hysteresis behavior appears, see the curve with $m = 10$. Unfortunately, the solution corresponding to the equation $q = 0$ cannot be obtained in these cases by the present method, since for one value of θ_w there are three solutions with different q. For this reason, the dashed line connecting two segments drawn with solid lines was not obtained numerically.

The two non-trivial solutions are illustrated in Fig. 4 for $a = 1$, $\ell = 10$ and $m = 20$. The temperature distributions (color plot) and isolines of the reaction rate ($\omega = 1$, 5, 10 and 20) correspond to the states indicated by triangles in Fig. 3. The temperature profiles are also represented in Figure 5, where the solid lines give the temperatures along the channel midplane, $y = 1/2$, and the dashed lines show the temperatures along the wall, at $y = 1$. It can be seen that in the center of the channel the temperature reaches values higher than the adiabatic flame temperature. This effect associated with the recirculation of heat through the conductive segment explains the large values for the operational flow rates.

The curves q versus θ_w are shown in Fig. 6 for a wider channel with $a = 3$ and several values of m for $\ell = 10$ (left plot) and $\ell = 15$ (right plot). It can be seen that the second critical value for the flow rate, m_{c2}, decreases with increasing channel width a but at the same time it increases with ℓ, for other parameters fixed. It is equal to $m_{c2} \approx 7.5$ for $\ell = 10$ and $m_{c2} \approx 11$ for $\ell = 15$. This result is consistent with the intuitive idea that an increase in the length of the recirculation

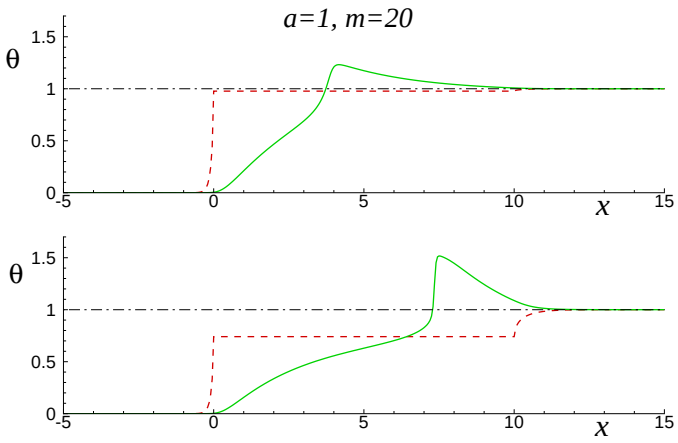

Figure 5: Temperature distributions along the lines $y = 1/2$ (solid curves) and along the wall $y = 1$ (dashed lines) for the states shown by open triangles in Fig. 3 for $a = 1$, $m = 20$ and $\ell = 10$.

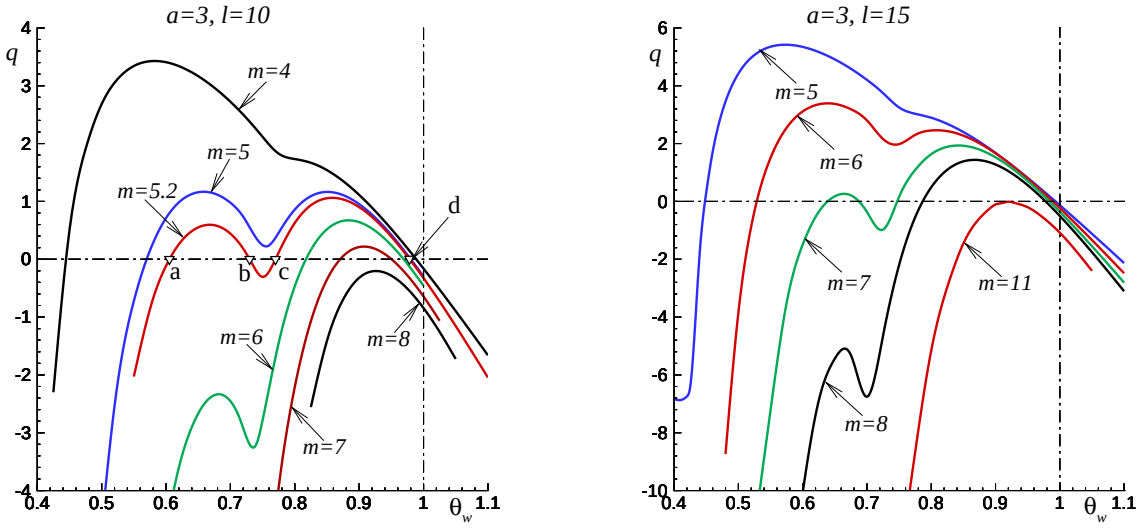

Figure 6: The response curves q versus θ_w computed for $a = 3$, $\ell = 10$ (left plot) and $a = 3$, $\ell = 15$ (right plot) and various m.

segment should enhance flame stabilization in the channel. Indeed, for $\ell \to 0$ it is difficult to expect this effect to be significant.

Interestingly, we observe in Fig. 6 that additional roots of the $q = 0$ equation appear at

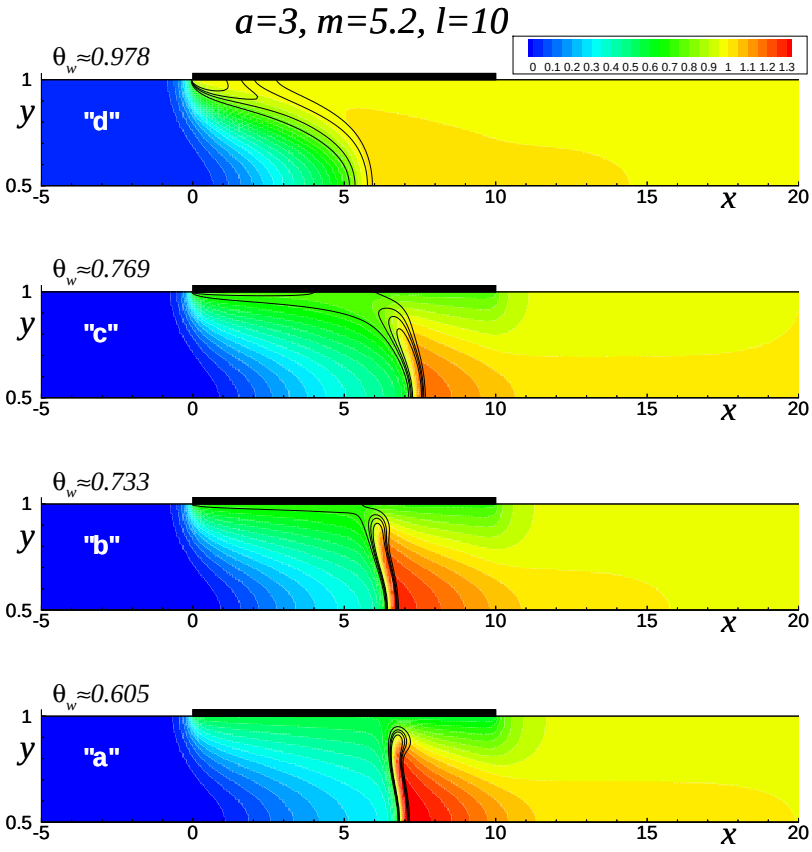

Figure 7: Flame structure corresponding to the states marked with open triangles in Fig. 6 (left plot), for $a = 3$, $m = 5.2$ and $\ell = 10$, for the temperature (color plot) and the reaction rate (isolines at $\omega = 1$, 2, 3 and 5).

intermediate values of m. This can be seen on the curves with $m = 5.2$ for $\ell = 10$ and $m = 7$ for $\ell = 15$. Thus, in these cases the number of non-trivial solutions increases to four. These solutions will be referred to as "a", "b", "c", and "d" in the following, as indicated in Fig. 6 (left plot) with open triangles.

The curves in Fig. 6 resemble the response curves behavior appearing for the steady-state flames stabilized in a flow around a circular cylinder of high thermal conductivity, as reported in [20]. In that study it was demonstrated that additional intermediate steady-state solutions also appeared at certain flow rates.

The flame structures corresponding to the roots of the $q = 0$ equation are shown in Fig. 7 for $\ell = 10$ and $m = 5.2$ using the temperature distribution (color plots) and reaction rate isolines ($\omega = 1$, 2, 3 and 5). These solutions are marked with open triangles in Fig. 6 (left plot) on the

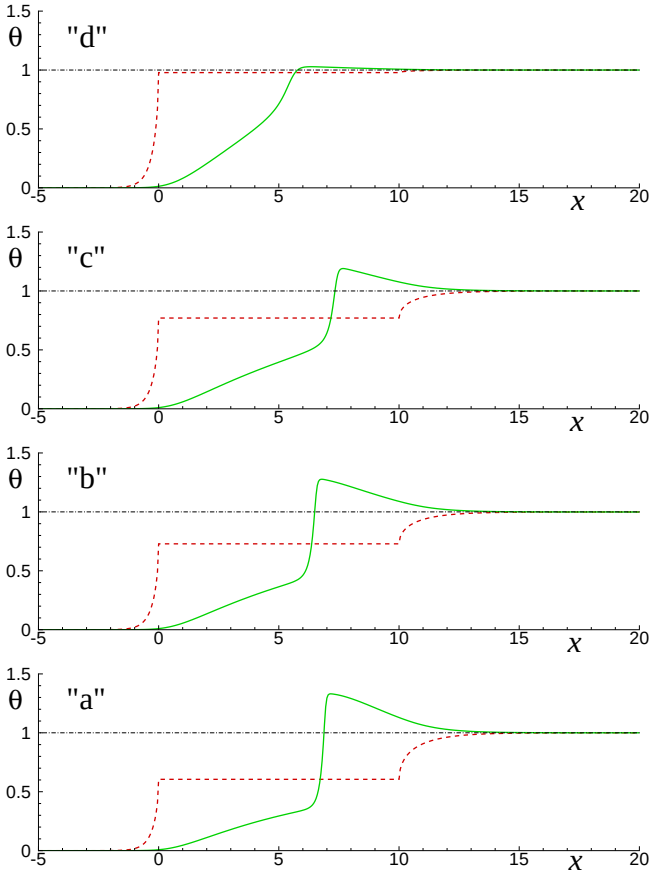

Figure 8: Temperature distributions in the center of the channel (solid lines) and along the wall (dashed lines) for solutions marked with open triangles in Fig 6 (left plot) for $m = 5.2$ and $\ell = 10$.

curve with $m = 5.2$. Figure 8 shows also the temperature distributions along the centerline of the channel (solid curves) and along the wall (dashed curves) for these four states.

The flame structures illustrated in Figs. 4 and 7 indicate that for all modes except for the mode with the hottest wall temperature (close to the adiabatic temperature), the combustion zone shown by the isoline of the reaction rate is located near the middle of the channel, while near the wall ω is small. This is due to the usually large Zel'dovich number, which leads to a sharp decrease in the reaction rate at temperatures below adiabatic temperature.

Interestingly, the flame position in the middle of the channel, defined as the maximum value of the reaction rate along this line, does not depend monotonically on the wall temperature. This dependence is shown in Fig. 9, where open circles show solutions marked as "a", "b", "c" and

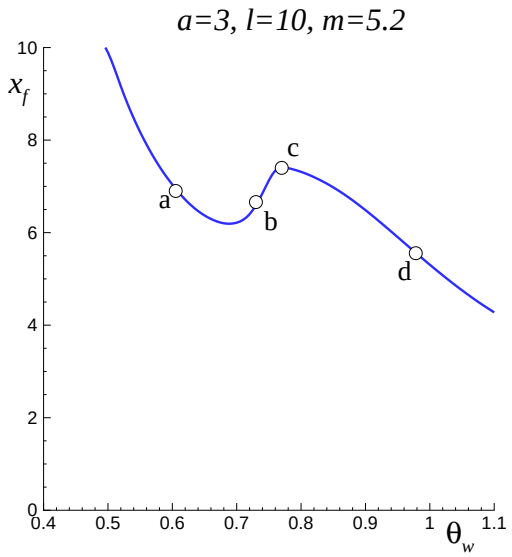

Figure 9: The flame position at the channel midplane as a function of the wall temperature for $a = 3$, $m = 5.2$ and $\ell = 10$. The open circles correspond to states "a", "b", "c" and "d" shown in Fig. 7 (the roots of $q = 0$).

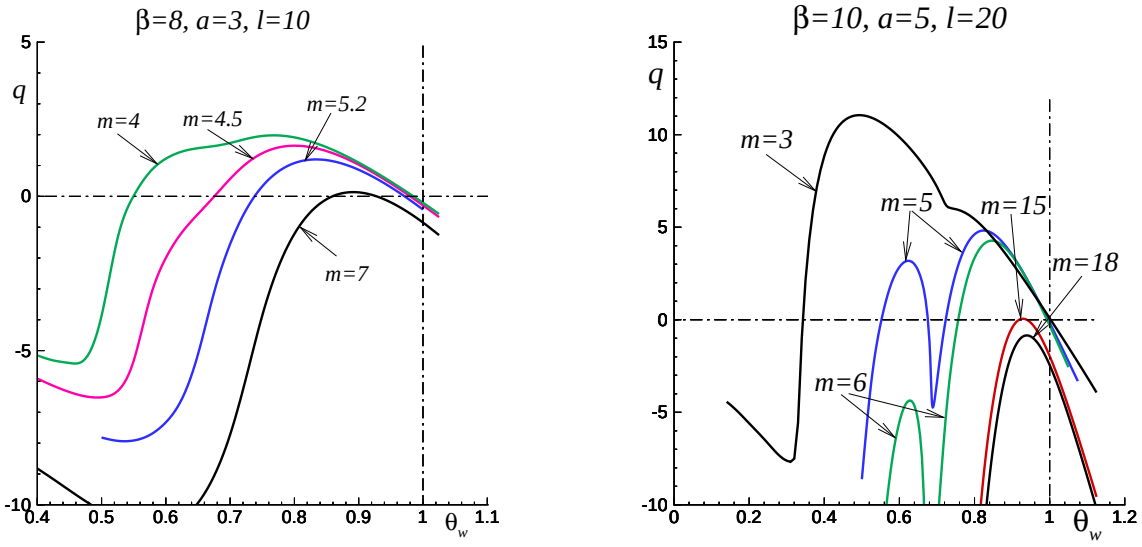

Figure 10: The response curves q versus θ_w computed for $\beta = 8$, $a = 3$, $\ell = 10$ (left plot) and $\beta = 10$, $a = 5$, $\ell = 20$ (right plot), and various values of m.

"d" corresponding to zero heat flux, $q = 0$, to the wall.

Numerical analysis reveals that the existence of additional solutions at intermediate values of the flow rate m is related to the Zel'dovich number. Figure 10 (left plot) shows the response curves obtained for $\beta = 8$, $a = 3$ and $\ell = 10$. It can be seen that no additional roots of the $q = 0$ equation appear. Thus, we can conclude that additional solutions will most likely appear for leaner mixtures corresponding to higher Zel'dovich numbers.

On the other hand, it should be noted that the emergence of additional steady-state solutions of the $q = 0$ equation at intermediate values of the wall temperature is a persistent trend. This takes place both as the channel is made wider and with an increase in the length of the heat-conducting wall segment. This is illustrated in Figure 10 (right plot) showing the response curves obtained for $a = 5$ and $\ell = 20$ (note that $\beta = 10$ was chosen for this plot).

5 Linear stability analysis

The linear stability analysis of the steady-state solutions presented in the previous section is now reported. Steady-state two-dimensional distributions of the temperatures and the mass fraction, all now denoted by subindex "0", are perturbed as usual with small perturbations

$$\begin{aligned} \theta &= \theta_0(x,y) + \epsilon\Phi(x,y)\exp(\lambda t), \\ Y &= Y_0(x,y) + \epsilon\Psi(x,y)\exp(\lambda t), \\ \theta_w &= \theta_{w0} + \epsilon\Phi_w\exp(\lambda t), \end{aligned} \tag{11}$$

where λ is a complex number, the real part of which represents the growth rate, and ϵ is a small amplitude. The linearized eigenvalue problem obtained when substituting Eq. (11) into Eqs. (1)-(4) reduces to finding non-trivial solutions of the two-dimensional system

$$\lambda\Phi = -mv(y)\frac{\partial\Phi}{\partial x} + \Delta\Phi + A\Phi + B\Psi, \tag{12}$$

$$\lambda\Psi = -mv(y)\frac{\partial\Psi}{\partial x} + Le^{-1}\Delta\Psi - A\Phi - B\Psi, \tag{13}$$

$$\lambda C\Phi_w = \int_0^\ell \left.\frac{\partial\Phi}{\partial y}\right|_{y=1} dx \tag{14}$$

where

$$A = \frac{\beta^3 Y_0}{2Leu_p^2[1+\gamma(\theta_0-1)]^2}\exp\left\{\frac{\beta(\theta_0-1)}{1+\gamma(\theta_0-1)}\right\}, \quad B = \frac{\beta^2}{2Leu_p^2}\exp\left\{\frac{\beta(\theta_0-1)}{1+\gamma(\theta_0-1)}\right\}$$

are both functions of x and y.

It is known that for a symmetric steady state investigated for stability, the existence of both symmetric and nonsymmetric perturbations is possible. This issue was studied in several publications, see e.g. [29, 34]. Within the framework of the diffusive-thermal model, non-symmetric perturbations are relevant for Lewis numbers different from unity and in channels of sufficient width. Since the present study is limited to narrow channels and the case with $Le = 1$, only symmetrical perturbations are assumed.

Equations (12)-(14) are to be solved subject to the following conditions

$$\forall x, \quad y = 1/2: \quad \partial\Phi/\partial y = \partial\Psi/\partial y = 0\,; \tag{15}$$

$$y = 1, \quad \begin{cases} x < 0,\, x > \ell: & \partial\Phi/\partial y = \partial\Psi/\partial y = 0\,, \\ 0 < x < \ell: & \Phi = \Phi_w, \quad \partial\Psi/\partial y = 0\,. \end{cases} \tag{16}$$

Since the eigenvalue problem is linear, we can normalize the eigenfunctions by setting $\Phi_w = 1$.

In the same manner as reported in [34] for flames in channels with adiabatic walls, the eigenvalue with a largest real part, or the main eigenvalue, was calculated. The method proposed in [34] was used to calculate this main eigenvalue. If the real part of this eigenvalue is positive, $\lambda_R = Re(\lambda) > 0$, then the steady-state is unstable, and conversely, if its real part is non-positive, $\lambda_R \leq 0$, the steady state is linearly stable. The imaginary part of this eigenvalue, $\lambda_I = Im(\lambda)$, represents the frequency of oscillations.

The parameter C appearing in Eq. (4) expresses the effective heat capacity of the bulk of the wall conductive material. When finding steady-state solutions in the previous section, this parameter could not affect the results. However, it is obvious that the properties of time dependent solutions, including the stability properties, depend on this parameter.

Figure 11 shows the real part of the main eigenvalues as functions of C computed for solutions "a", "b", "c" and "d" indicated by the open triangles in Fig. 6. It should be noted that since the eigenvalue decreases with increasing C, it is convenient to plot $\lambda_R C$ along the vertical axis. The solid lines in the figure correspond to purely real eigenvalues, and only for the segment drawn by a dotted line (solution "b") the imaginary part is non-zero. The transition points from the complex eigenvalue to the purely real one for solution "b" are indicated by open circles. By chance, one of these points lies very close (almost above) to the eigenvalue curve of the solution "a" which is purely real.

When studying linear stability, a qualitative method based on the slope of the response curves is often used. For example, for the curve shown in Fig. 6 for $m = 5.2$, solutions "a" and "c"

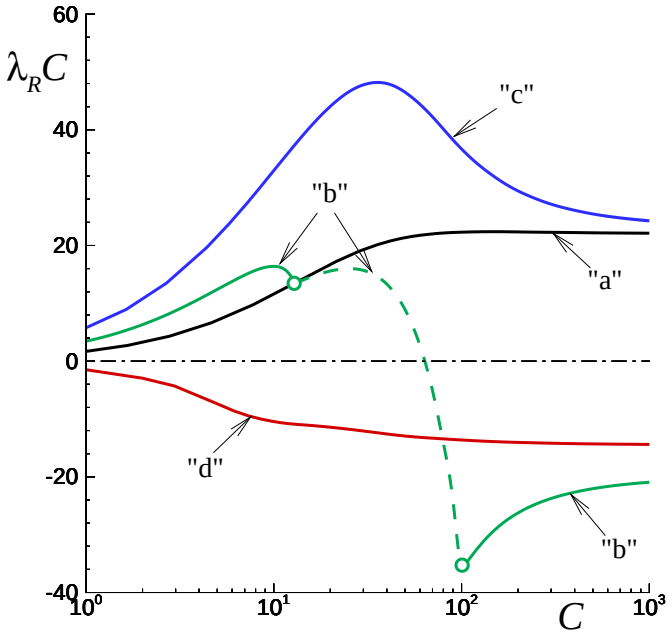

Figure 11: The real part of the main eigenvalue as a function of parameter C (the values of $\lambda_R C$ are drawn along the vertical axis) for "a", "b", "c" and "d" solutions calculated for $m = 5.2$, $a = 3$ and $\ell = 10$. The solid curves represent the purely real eigenvalues ($\lambda_I \equiv 0$) and a dashed line segment shown for the "b" solution shows the eigenvalues with $\lambda_I \neq 0$. The transition points from complex to purely real values are marked with open circles. (Comment: one of the circles corresponding to the "b" curve overlaps with the λ-curve for the "a" solution which is entirely real).

would be declared unstable. Indeed, with a random increase in the wall temperature θ_w the heat flux to the heat exchange segment decreases, according to the response curve, and, thus, θ_w should decrease. Conversely, when the wall is randomly cooled then, according to the response curve, the heat flux q increases and the wall heats up.

The results presented in Fig. 11 show that the steady-state solutions "a" and "c" are always unstable ($\lambda_R > 0$), while the solution "d" is always stable ($\lambda_R < 0$). This is in agreement with the qualitative consideration described above. However, for the steady-state solution "b", the above method does not work: the negative slope of the response curve at "b" would lead to the conclusion that "b" is stable. However, the numerical calculations show that for suffi-

ciently small values of C this solution is unstable, while for sufficiently large C the "b" solution becomes stable.

Figure 11 also shows that at $C \gg 1$, the values of λC tend to constants. This can also be seen also from Eqs. (12)-(14). Indeed, at $C \to \infty$ it is convenient to re-normalize the eigenvalue as $\tilde{\lambda} = \lambda C$. Then, the left hand sides of Eqs. (12)-(13) become small, of order $\sim 1/C$ and given that $C \gg 1$, these terms can be neglected in the first approximation. This means that the functions Φ and Ψ become independent of λ. After this, Eq. (14) gives

$$\tilde{\lambda} = \int_0^\ell \partial\Phi/\partial y\big|_{y=1} dx \,,$$

which is independent of C.

6 Time-dependent calculations

Time-dependent calculations of Eqs. (1)-(4) were carried out for several initial conditions. First, the following initial state was chosen,

$$t = 0: \quad \theta = Y - 1 = 0, \quad \theta_w = \theta_{w0} \,, \tag{17}$$

which corresponds to the flow of a cold fresh mixture in the channel and instantaneous heating of the conductive wall segment up the temperature $\theta_w = \theta_{w0}$. Figure 12 illustrates snapshots of the flame dynamics obtained with $\theta_{w0} = 0.9$.

The time histories of θ_w for $\theta_{w0} = 0.8$ and $\theta_{w0} = 0.9$ are shown in Fig. 13 for $m = 5.2$. Solid lines correspond here to $C = 500$, dashed lines to $C = 200$ and the dash-dotted line to $C = 100$ (only for $\theta_{w0} = 0.9$). It can be seen that with a higher initial temperature of the wall, the final state of the system is the state "d", and for a colder initial temperature, the system reaches the state "b". This happens for both $C = 500$ and $C = 200$. However, for $C = 100$ (dash-dotted line), extinction occurs. This result confirms that the existence of two stable steady-states for the same values of the parameters is not a numerical artifact. These two states can be obtained under fairly simple initial conditions.

In order to investigate the dependence of the dynamical properties of the "b" state on the parameter C, the following calculations were carried out. We chose as initial conditions the distributions of the temperature and mass fraction for the "b" state obtained by the steady-state method (assuming $\partial/\partial t \equiv 0$) or the time-dependent method with large C. Thereafter, a small

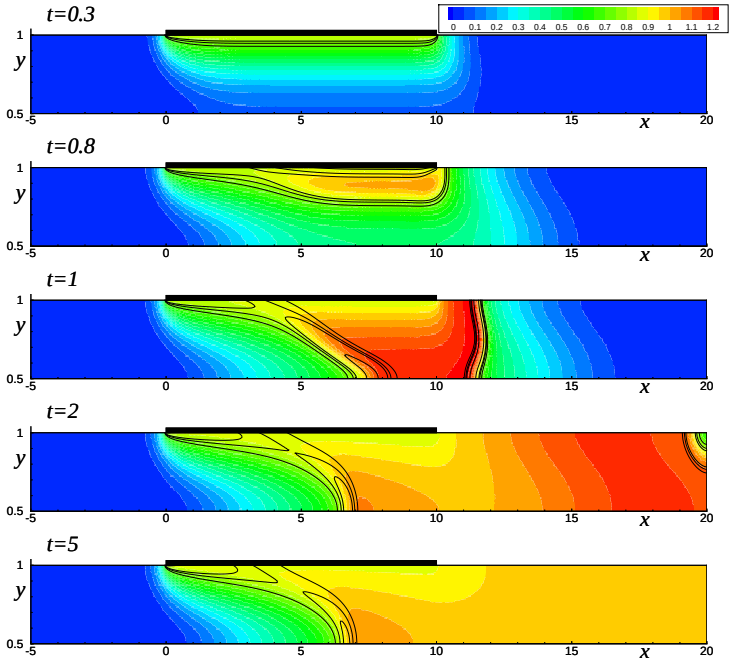

Figure 12: Snapshots for the ignition process from a intracutaneously heated wall up to $\theta_{w0} = 0.9$ in an initially cold channel, for $m = 5.2$, $a = 3$, $\ell = 10$ and $C = 200$.

perturbation was added to the wall temperature only. The initial conditions obtained in this way were used to carry out calculations for different values of the parameter C. Recall that the stable-unstable boundary for the "b" solution was found near $C_* \approx 63$ for $m = 5.2$, $a = 3$ and $\ell = 10$.

The time history for the wall temperature is shown in Fig. 14 for different values of the parameter C and for two initial wall temperatures θ_{w0}. The latter are indicated in Fig. 14 by open circles. The value for the unperturbed wall temperature corresponding to the steady state "b" is shown with a horizontal dash-dotted line. One can see that for an initial wall temperature $\theta_{w0} = 0.75$ (the wall temperature perturbation is about $\%2$), the system returns to state "b" for $C = 100$ and 80, while for $C = 75$ there is no return to state "b". However, for $\theta_{w0} = 0.74$ (the wall temperature perturbation $\lesssim \%1$), the system approaches the steady-state "b" for $C = 70$. For the same initial wall temperature and for $C = 60$ (below the threshold value $C_* \approx 63$ of the "b" state), periodic small-amplitude oscillations of the wall temperature take place. When the parameter C decreases, e.g. to $C = 55$, the amplitude of these oscillations increases.

It is interesting to note that by initiating calculations from the same initial conditions ($\theta_{w0} = 0.74$) but with smaller values for parameter C, the Feigenbaum's cascade of period doubling

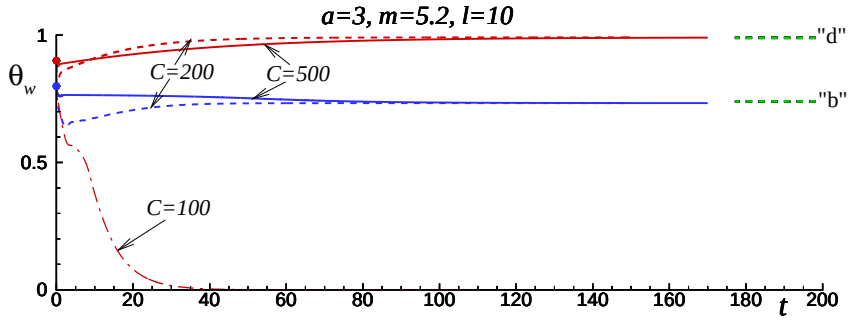

Figure 13: Time history of the wall temperature for ignition from $\theta_{w0} = 0.8$ and $\theta_{w0} = 0.9$: solid lines - $C = 500$, dotted lines - $C = 200$, a dash-dotted line - $C = 100$ (only for $\theta_{w0} = 0.9$), for $a = 3$, $m = 5.2$ and $\ell = 10$.

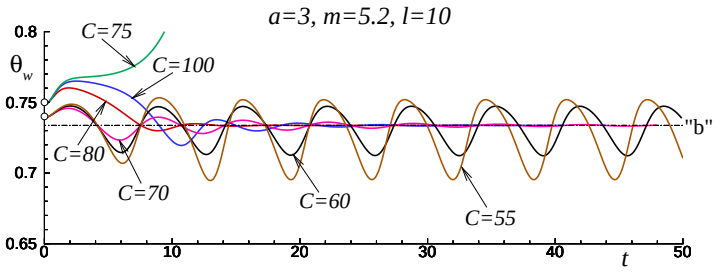

Figure 14: Time history of the wall temperature after the perturbation of the steady-state solution "b" (indicated with a dash-dotted line) for different values of the parameter C and θ_{w0} (indicated with open circles), all curves for $a = 3$, $m = 5.2$ and $\ell = 10$.

bifurcations takes place, leading ultimately to a chaotic regime. Figure 15 illustrates the dynamics of the wall temperature for $C = 48$, 47.3 and 45.5. With a decrease to $C = 45.5$, the wall temperature dynamics apparently becomes chaotic, as the bottom plot of Fig. 15 illustrates.

We do not present here the time histories of the wall temperature related to the intermediate period doubling events that occur during the transition to chaotic dynamics, since it is difficult to follow these events from such plots. Instead, the flame dynamics is illustrated with the first return map technique. Using the dependence of the wall temperature on time, the series of local maxima of θ_w are identified, $\{\theta_w^{(n)}, n = 1, 2, \dots\}$, where n is the maximum number. The dependence $\theta_w^{(n+1)}$ versus $\theta_w^{(n)}$ is plotted in Fig. 16. These plots were created using $n \gtrsim 10$ after the starting of simulations, in order to allow the flame dynamics to approach the corresponding attractor.

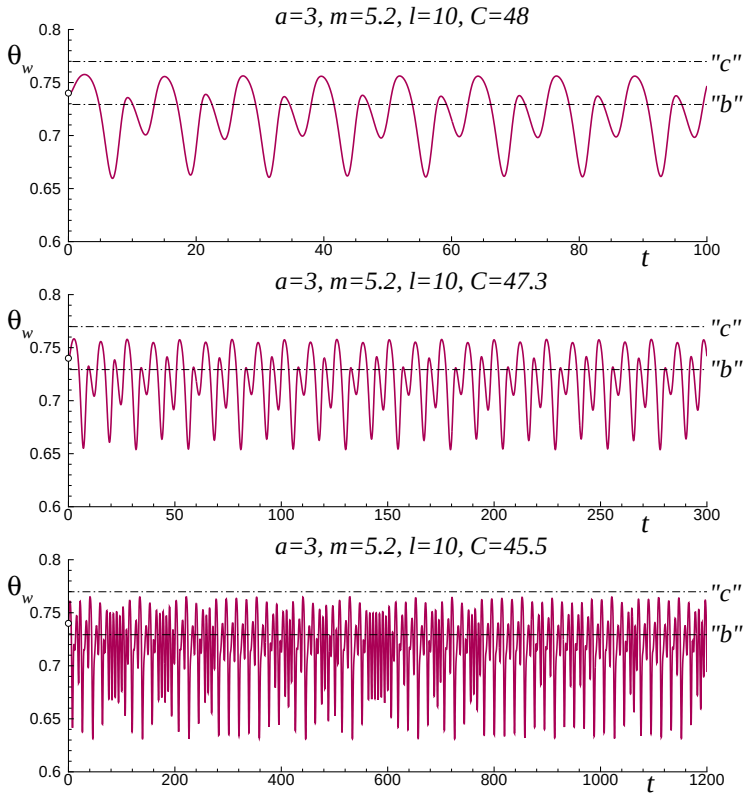

Figure 15: Time histories of the wall temperature after the perturbation of θ_w calculated for $a = 3$, $m = 5.2$ and $\ell = 10$ and various decreasing values of C. The horizontal dash-dotted lines indicate the steady states "b" and "c", the vertical dashed lines on the top and middle plots show the oscillation period.

Figure 16 (upper left) indicates that for $C = 47.3$ there are four local maxima for θ_w within one period. For $C = 47.2$ the first return map consists of four continuous segments. It is interesting to note that with a further decrease in the C parameter, a second branch appears on the return map. This is especially evident in Fig. 16 (lower right), where the two branches are marked with dashed lines.

Intermittency is well known as the irregular alternation of phases of apparently periodic and chaotic dynamics, see [35]. Intermittent behavior has been reported recently in the description of a combustion wave propagating in a narrow sample of energetic material [36]. The intermittency effect was also observed for the time dependent behavior of the wall temperature. Fig. 17 shows the different intervals of the time-history of θ_w calculated for $C = 45.5$. The phases of apparently periodic behavior are indicated with dashed-line circles. It can be seen in the up-

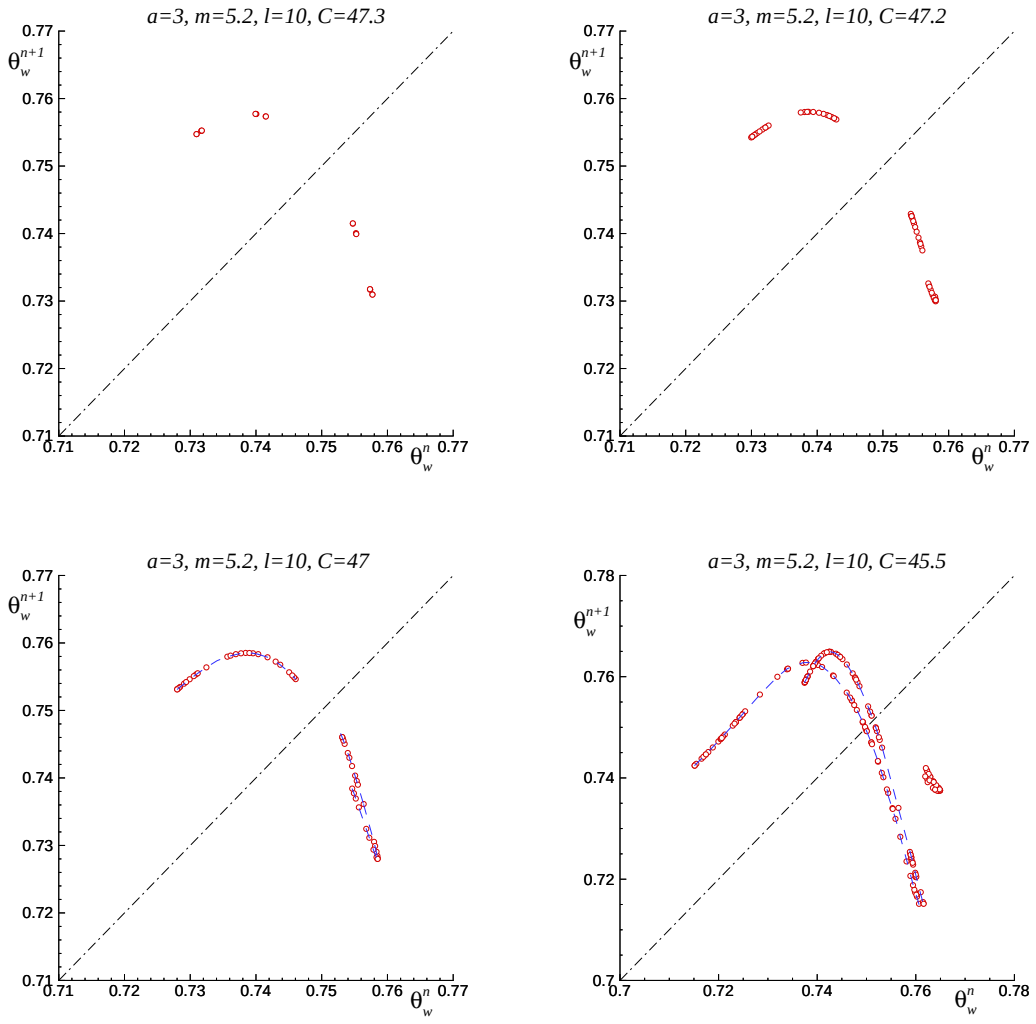

Figure 16: First return maps for the wall temperature θ_w calculated for $a = 3$, $m = 5.2$, $\ell = 10$ and various values of C.

per figure that simple oscillations alternate with chaotic behavior, while in the lower figure the oscillations are more complex in the interval of periodic behavior.

Numerical simulations show, however, that at even smaller values of C, the amplitude of oscillations increases and the system moves toward the stable state ”e”. This can be seen in Fig. 18 where the top plot presents the wall temperature and the bottom plot shows the total heat flux into the wall. The top plot indicates that as soon as the instantaneous wall temperature value exceeds that of the (unstable) ”c” mode, a transition to the steady state ”d” occurs. An interesting detail is also that the chaotic oscillations around the ”b” state can continue for a considerable

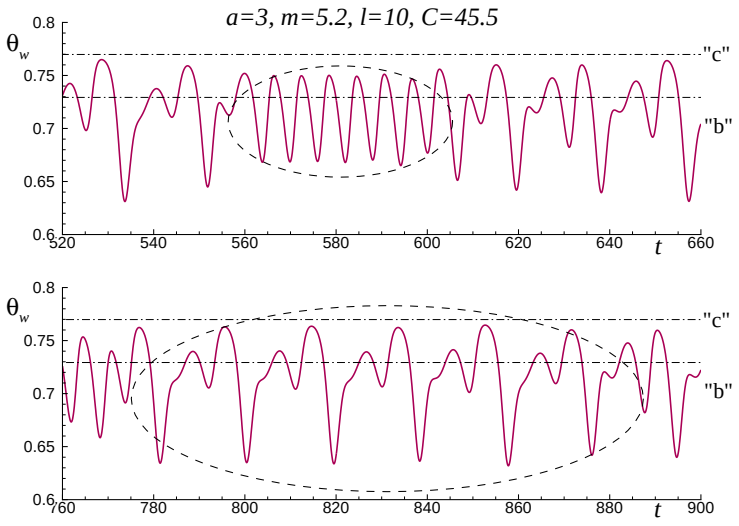

Figure 17: Intermittency intervals in the wall temperature dynamics: the phases of apparently periodic dynamics are indicated with dash-lines circles, for $C = 45.5$.

time before the transition to a (stable) steady state occurs.

7 Discussion and conclusions

When studying the structure and dynamics of flames in channels, the modeling of the flame-wall interaction is often simplified. Two of the most common approximations are the adiabatic limit, when the heat flux to the wall is assumed to be zero, and the isothermal wall approximation, when the wall temperature is assumed to be constant and equal to the ambient temperature. An intermediate approximation between these two limits is to assume that the heat exchange between the wall and the flame follows a linear law, so that the heat flux to the wall is proportional to the difference between the internal and external wall temperatures. This is the so-called thin-wall approximation, when the temperature distribution inside the wall is assumed to be linear with respect to the normal-to-wall direction. The limiting cases for this approximation result in the adiabatic or isothermal temperature wall boundary conditions.

However, one can easily imagine a situation where at least a part of the wall surrounding the combustion zone is made from a highly conductive material, for example a metal-like material, leading to a uniform wall temperature. Typically, the thermal conductivity of of such substances is several hundred times higher than that of the gas phase, and because they are convenient

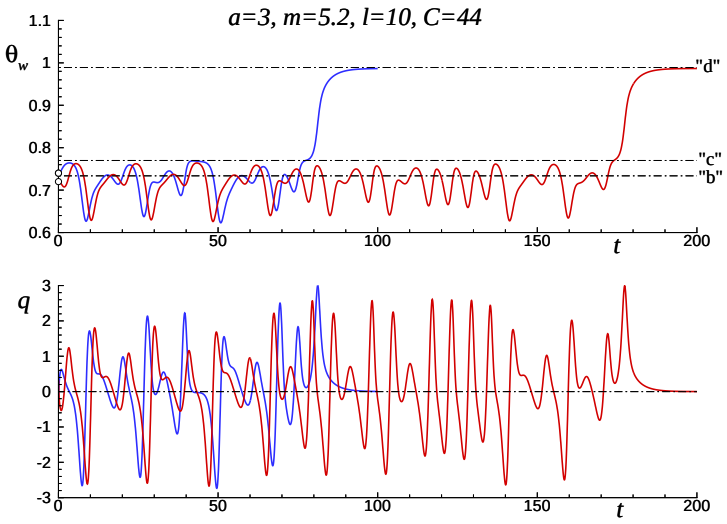

Figure 18: Time histories of the wall temperature (upper plot) the heat flux to the wall (lower plot) calculated for $a = 3$, $m = 5.2$, $\ell = 10$ and $C = 44$ after the perturbations of θ_w (marked with open circles in the upper plot). The horizontal dash-dotted lines indicate the steady states "b", "c", and "d" in the upper plot.

materials for the design of combustion devices, this possibility cannot be ignored, especially when analyzing small-scale devices. The use of highly conductive materials also makes possible to enhance the effect of heat recirculation in the system under consideration.

This work presents an attempt to study numerically this kind of situation. We investigate a narrow channel in which a wall segment is composed of a highly conductive material, which results in temperature uniformity within this segment. The description of this geometry contains many parameters, so a complete detailed study of the influence of all of them is not possible in a theoretical work. The presentation is limited to selected cases, which, in our opinion, may be of a more general nature.

The asymptotic limit of a large ratio of the thermal conductivities of the wall and the gas makes it possible to simplify significantly the procedure of finding steady-state solutions, since by setting the wall temperature the heat flux into the wall, q, is calculated directly. If the heat-conducting wall segment separates adjacent channels (or it is isolated from the environment), then the condition for the steady-state mode becomes $q = 0$. It is also easy to take into account possible heat losses from this segment, if any.

Although the physical situation does not change for a finite (but large) ratio of thermal con-

ductivities, the procedure for finding steady-state regimes becomes more complicated due to the need to calculate the inhomogeneous temperature field inside the wall and the temperature distribution in the adjacent channel (in the case of a periodic system of micro-burner channels). Indeed, the symmetry condition in the middle of the heat-conducting wall cannot be set, and the calculation of the variable distributions in the adjacent channel is unavoidable. Thus, the study of the limiting case with an infinite ratio of thermal conductivities is extremely useful for a qualitative and quantitative understanding of the combustion process.

To analyze the problem, a simple diffusive-thermal model is chosen. Since the effects under study are related to the process of heat exchange between the flame and the wall, and in the case of narrow channels, it is expected that this approximation does not take the results very far from reality. The use of this simplified model has the advantage of permitting the linear stability study of the obtained stationary solutions, as well as the computation of time-dependent solutions at low cost.

The simulation results show that the highly conductive wall segment acts as a flame holder. Additionally, the system presents multiple solutions for a wide range of mixture flow rates, there are at least two non-trivial solutions for steady-state regimes. This number can increase to four as the channel width and the length of the highly conductive segment increase.

Numerical analysis of the linear stability of the found steady-state modes reveals that some of them are always stable, but the stability of some others depends on the parameters characterizing the system as a whole, but not affecting the steady state solutions. Such a parameter is the effective heat capacity of the conductive wall segment represented by the C parameter in Eq. 4). It is also shown that the Feigenbaum's cascade of period doubling bifurcations can appear leading to a chaotic dynamics. Although the initial conditions used to obtain such solutions were of a special type (it was assumed that the parameter C instantly changes its value at the initial moment), the Feigenbaum cascade preceding the appearance of chaotic dynamics might possibly also appear using other initial conditions.

As mentioned above, the system under study can be considered as part of a small-scale device with heat recirculation, when the channels are separated by walls made of a highly conductive material. All the results obtained in this work can be transferred to this case. However, it should be noted that the relaxation of some of the assumptions made in this study, for example, the symmetry of the flame in the channel relative to its middle, can lead to additional effects that would require further investigation.

Acknowledgement

This work was financed by project #PID2019-108592RB-C42 / AEI / 10.13039/501100011033.

References

[1] A.C. Fernández-Pello, Micropower generation using combustion: issues and approaches, *Proc. Combust. Inst.* 29 (2002) 883-899.

[2] Y. Ju, K. Maruta, Microscale combustion: technology development and fundamental research, *Prog. Energy Combust. Sci.* 37 (2011) 669-715.

[3] N.S. Kaisare , D.G. Vlachos , A review on microcombustion: fundamentals, de-vices and applications, *Prog. Energy Combust. Sci.* 38 (3) (2012) 321359 .

[4] J.L. Ellzey, E.L. Belmont, C.H. Smith, Heat recirculating reactors: Fundamental research and applications, *Prog. Energy Combust. Sci.* 72 (2019) 32-58.

[5] S.A. Lloyd, F.J. Weinberg, A burner for mixtures of very low heat content, *Nature* 251 (1974) 47-49.

[6] S.A. Lloyd, F.J. Weinberg, Limits to energy release and utilisation from chemical fuels, *Nature* 257 (1975) 367-370.

[7] A.R. Jones, S.A. Lloyd, F.J. Weinberg, Combustion in heat exchangers, *Proc. R. Soc. Lond. A.* 360 (1978) 97-115.

[8] Y. Ju, C.W. Choi, An analysis of sub-limit flame dynamics using opposite propagating flames in mesoscale channels, *Combust. Flame* 133 (2003) 483-493.

[9] R.V. Fursenko, S. S. Minaev, Flame stability in a system with counterflow heat exchange, *Combust. Explos. Shock Waves* 41(2) (2005) 133-139.

[10] I. Schoegl, J.L. Ellzey, Superadiabatic combustion in conducting tubes and heat exchangers of finite length, *Combust. Flame* 151 (2007) 142-159.

[11] V.N. Kurdyumov, D. Fernández-Galisteo, C. Jiménez, Superadiabatic small-scale combustor with counter-flow heat exchange: Flame structure and limits to narrow-channel approximation, *Combust. Flame* 222 (2020) 233-241.

[12] J. Bosch, D. Fernández-Galisteo, C. Jiménez, V.N. Kurdyumov, Analytical study of superadiabatic small-scale combustors with a two-step chain-branching chemistry model: lean burning below the flammability limit, *Combust. Flame* 235, (2022) 11173.

[13] T. Takeno, K. Sato, An excess enthalpy flame theory, *Combust. Sci. Tech.* 20 (1979) 73-84.

[14] B. Deshaies, G. Joulin, Asymptotic study of an excess-enthalpy flame, *Combust. Sci. Tech.* 22 (1980) 281-285.

[15] J. Buckmaster, T. Takeno, Blow-off and flashback of an excess enthalpy flame, *Combust. Sci. Tech.* 25 (1981) 153-158.

[16] T. Takeno, K. Sato, K. Hase, A theoretical study on an excess enthalpy flame, *Proc. Combust. Inst.* 18 (1981) 465-472.

[17] M.A.A. Mendes, J.M.C. Pereira, J.C.F. Pereira, A numerical study of the stability of one-dimensional laminar premixed flames in inert porous media, *Combust. Flame* 153 (2008) 525-539.

[18] V.N. Kurdyumov, D. Fernández-Galisteo, C. Jiménez, Asymptotic study of premixed flames in inert porous media layers of finite width: Parametric analysis of heat recirculation phenomena, *Combust. Flame* 241 (2022) 112109.

[19] S. Berger, F. Duchaine, L.Y.M. Gicquel, Bluff-body thermal property and initial state effects on a laminar premixed flame anchoring pattern, *Flow Turb. Combust.* 100 (2018) 561-591.

[20] V.N. Kurdyumov, C. Jiménez, Flame stabilisation by a highly conductive body: multiple steady-state solutions and time-dependent dynamics, *Combust. Theor. Modell.* 26 (2021) 669-685.

[21] D.J. Diamantis, E. Mastorakos, D.A. Goussis, Simulations of premixed combustion in porous media, *Combust. Theory Modell.* 6 (2002) 383-411.

[22] P.-A. Masset, O. Dounia, L. Selle, Fully explicit formulae for flame speed in infinite and finite porous media, *Combust. Theory Modell.* 25 (2021) 785-812.

[23] V. N. Kurdyumov, J.-M. Truffaut, J. Quinard, A. Wangher, G. Searby, Oscillations of premixed flames in tubes near the flashback conditions *Combust. Sci. Tech.* 180 (2008) 731-742.

[24] D.K. Lee, K. Maruta, Heat recirculation effects on flame propagation and flame structure in a mesoscale tube, *Combust. Theory Modell.* 16 (2012) 507-536.

[25] G. Pizza, Ch.E. Frouzakis, J. Mantzaras, A.G. Tomboulides, K. Boulouchos, Dynamics of premixed hydrogen/air flames in microchannels, *Combust. Flame* 152 (2008) 433-450.

[26] G. Pizza, Ch.E. Frouzakis, J. Mantzaras, A.G. Tomboulides, K. Boulouchos, Dynamics of premixed hydrogen/air flames in mesoscale channels, *Combust. Flame* 155 (2008) 2-20.

[27] V.N. Kurdyumov, G. Pizza, Ch.E. Frouzakis, J. Mantzaras, Dynamics of premixed flames in a narrow channel with a step-wise wall temperature,*Combust. Flame* 156 (2009) 2190-2200.

[28] G.P. Gauthier, G.M.G. Watson, J.M. Bergthorson, An evaluation of numerical models for temperature-stabilized CH4/Air flames in a small channel, *Combust. Sci, Thech.* 184 (2012) 850-868.

[29] V.N. Kurdyumov, C. Jiménez, Propagation of symmetric and non-symmetric premixed flames in narrow channels: Influence of conductive heat-losses, *Combust. Flame* 161 (2014) 927-936.

[30] G.P. Gauthier, G.M.G. Watson, J.M. Bergthorson, Burning rates and temperatures of flames in excess-enthalpy burners: A numerical study of flame propagation in small heat-recirculating tubes, *Combust. Flame* 161 (2014) 2348-2360.

[31] G.P. Gauthier, J.M. Bergthorson,Effect of external heat loss on the propagation and quenching of flames in small heat-recirculating tubes, *Combust. Flame* 173 (2016) 27-38.

[32] K. Bioche, L. Vervisch, G. Ribert, Premixed flame-wall interaction in a narrow channel: impact of wall thermal conductivity and heat losses, *J. Fluid Mech.* 856 (2018) 5-35.

[33] K. Bioche, G. Ribert, L. Vervisch, Simulating upstream flame propagation in a narrow channel after wall preheating: Flame analysis and chemistry reduction strategy, *Combust. Flame* 200 (2019) 219-231.

[34] V.N. Kurdyumov, Lewis number effect on the propagation of premixed flames in narrow adiabatic channels: Symmetric and non-symmetric flames and their linear stability analysis, *Combust. Flame* 158 (2011) 1307-1317.

[35] Y. Pomeau , P. Manneville , Intermittent transition to turbulence in dissipative dynamical systems, *Commun. Math. Phys.* 74 (1980) 189-197 .

[36] V.N. Kurdyumov, V.V. Gubernov, Propagation of a reaction front in a narrow sample of energetic material with heat losses: Chaotic regimes, extinction and intermittency, *Combust. Flame* 191 (2018) 19-31.